Supplement of Atmos. Chem. Phys., 20, 6055–6080, 2020
https://doi.org/10.5194/acp-20-6055-2020-supplement

Atmospheric Chemistry and Physics
Open Access
EGU

Supplement of

Heterogeneous oxidation of amorphous organic aerosol surrogates by O_3, NO_3, and OH at typical tropospheric temperatures

Jienan Li et al.

Correspondence to: Daniel A. Knopf (daniel.knopf@stonybrook.edu)

S1. Axial temperature profile in flow reactor

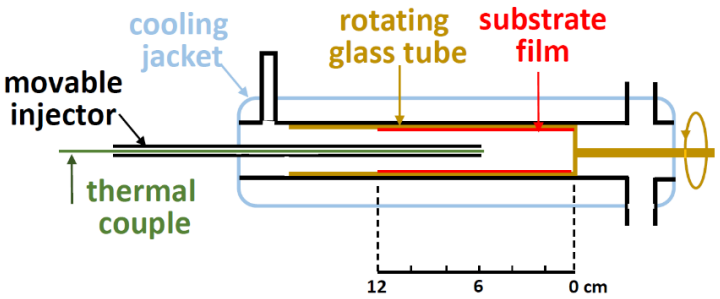

Figure S1. Measurement of the axial temperature in the flow reactor.

The flow reactor is designed to conduct uptake experiments in the temperature range of 313.15 K to 213.15 K. To ensure minimal axial temperature gradients, we measured the temperature along the flow reactor using a thermocouple wire at the tip of the injector. As the thermocouple is moved in tandem with the movable injector, the temperature along the flow tube axis is recorded. We measured the temperature profile for different flow rates (50, 200, 500, 1000 and 2000 cm^{-3} min^{-1}, STP) at ~293 K, 273 K, 243 K and 213 K. Table A1 shows the temperature values at different distances for the coldest applied temperature (211 K) and corresponding pressures under different flow conditions. As can be seen, for the first 6 cm of the reactive substrate, the temperature is equal within 0.5 K including the fastest applied flows of 2000 cm^{-3} min^{-1} (STP). Significant deviation from desired temperature occurs only beyond 10 cm. For slower flow rates, the flow reactor exhibits uniform temperature. In most of the presented uptake experiments, the total flowrate in the flow reactor is below 1000 cm^{-3} min^{-1} (STP), and thus the temperature change is smaller than 1 K within 10 cm of the reactive film length. Therefore, no significant effects of the temperature gradient on substrate phase state and reaction kinetics are expected.

Table S1. Axial temperature measurements for various flow conditions at T = 211 K. The temperature accuracy is ±0.2 K with a resolution of 0.1 K for all measurements. P_{FR} represents pressure in the flow reactor.

Distance	50 sccm	200 sccm	500 sccm	1000 sccm	2000 sccm
2 cm	211 K	210.9 K	211 K	210.9 K	211 K
4 cm	211 K	211 K	211 K	210.9 K	211.3 K
6 cm	211 K	211 K	211 K	211 K	211.7 K
8 cm	211 K	211 K	211 K	211.1 K	212.5 K
10 cm	211 K	211 K	211 K	211.5 K	215 K
12 cm	211 K	211.1 K	211.5 K	213.8 K	222.1 K
P_{FR}	2.16 hPa	1.7 hPa	2.32 hPa	3.54 hPa	5.44 Pa

S2. Measurement of the water content in the organic substrate films

The water content in the organic film substrate was determined using an ultra-microbalance with an accuracy of 0.2 µg (Mettler Toledo XP2U). Six drops of organic/water solution are applied to a glass slide with a 2 µL pipette. After drying the droplets following the same procedure as film preparation in the uptake experiments, the thickness of the resulting films is about 50-100 µm, like the film substrates in the uptake experiments. The film thickness can be measured using a microscope. The water content is derived by the mass difference before and after the drying procedure, expressed by the following equation:

$$w\% = \frac{m_{\text{final}} - m_{\text{initial}} \times R_{\text{org}}}{m_{\text{final}}} \times 100\% \,, \qquad \text{(S1)}$$

where m_{final} is the mass of the substrate film after the drying procedure, m_{initial} is the initial mass of the solution drops, and R_{org} is the initial mass ratio of the organic component to water in the solution. Levoglucosan, glucose and xylitol are non-volatile. The vapor pressure of 1,2,6 hexanetriol is ~ $(3.82 \pm 1.16) \times 10^{-4}$ Pa (Lv et al., 2019) and thus can be ignored compared to water with a vapor pressure of 2.34 kPa at 293.15 K. As shown in Table S2, the water content of applied films ranges from (10.33±0.54) % to (16.02±0.79) % at room temperature, indicating that water molecules can still be trapped in the substrate films after the drying process.

Table S2. Estimated water concentration in the applied substrate films.

substrate	Initial solute concentration / wt%	Organic mass ratio	Estimated water content / wt%
LEV	5	1	13.6±0.3
LEV/XYL	5	1:1	16.0±0.8
GLU	10	1	13.2±1.6
GLU/HEX	10	4:1	13.8±1.2

Table S3. Water concentration in the levoglucosan film substrates. Five samples are evaluated resulting in an average water content of 13.56 wt% and standard deviation σ = 0.33 wt%.

#	m_{final} / mg	m_{initial} / mg	R_{org}	Concentration / wt%
	0.6766	11.6577	0.05	13.85
2	0.7105	12.2391	0.05	13.87
3	0.7259	12.5564	0.05	13.51
4	0.7009	12.1216	0.05	13.52
5	0.6864	11.9375	0.05	13.04

Table S4. Water concentration in LEV/XYL film substrates with mass ratio of 1:1. Five samples evaluated resulting in an average water content of 16.02 wt% and standard deviation σ = 0.79 wt%.

#	m_{final} / mg	$m_{initial}$ / mg	R_{org}	Concentration / wt%
1	0.7262	12.0218	0.05	17.22
2	0.6929	11.6323	0.05	16.06
3	0.7028	11.9386	0.05	15.06
4	0.7229	12.1855	0.05	15.72
5	0.7114	11.9457	0.05	16.04

Table S5. Water concentration in film substrates of glucose. Six samples are evaluated resulting in an average water content of 13.17 wt% and standard deviation σ = 1.58 wt%.

#	m_{final} / mg	$m_{initial}$ / mg	R_{org}	Concentration / wt%
1	1.4208	12.0855	0.1	14.94
2	1.4000	12.2318	0.1	12.63
3	1.4599	12.4411	0.1	14.78
4	1.4371	12.3182	0.1	14.28
5	1.3754	12.1838	0.1	11.42
6	1.3738	12.2300	0.1	10.98

Table S6. Water concentration in substrate films of GLU/HEX with mass ratio of 1:4. Five samples are evaluated resulting in an average water content of 13.84 wt% and standard deviation σ = 1.24 wt%.

#	m_{final} / mg	$m_{initial}$ / mg	R_{org}	Concentration / wt%
1	1.4837	12.4658	0.0999	15.98
2	1.4070	12.1748	0.0999	13.47
3	1.4224	12.3041	0.0999	13.50
4	1.4757	12.5525	0.0999	14.94
5	1.4701	12.8476	0.0999	12.61
6	1.4634	12.8002	0.0999	12.53

S3. Glass transition estimation using the poke-flow technique

T_g can be estimated by monitoring the flowing and shattering of the substrate films while lowering the temperature of the substrate. From a starting temperature T which is slightly higher (e.g., 10 K) than the predicted T_g, we poke the film to determine its phase. If the film does not shatter, the temperature of the cell is lowered by 3 K. After 5 mins at this new temperature, the substrate is poked again to monitor potential shattering. For each substrate, we examined the phase state at least six times and calculated the average to yield the estimated T_g value. Structures in Figs. S2-S7 that are not in focus are from minor superficial scratches of the silver sample holder within the temperature-controlled cooling stage. Figures S2 and S3 show images of shattering substrates and corresponding T_g estimates for GLU and GLU/HEX substrate mixtures.

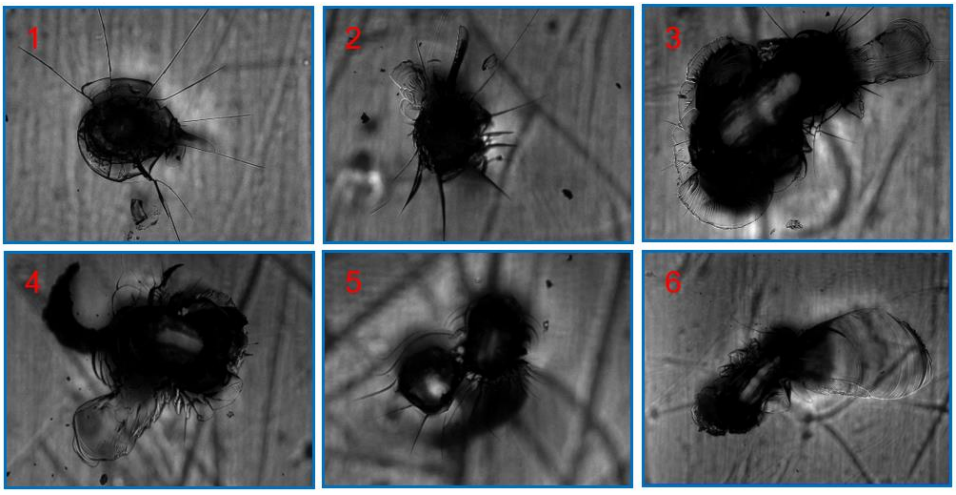

Figure S2. T_g estimation using poke-flow technique. Shattering of GLU films. The shattering temperatures are 277 K, 273 K, 271 K, 272 K, 275 K, 270 K. The average is (273 ± 2) K.

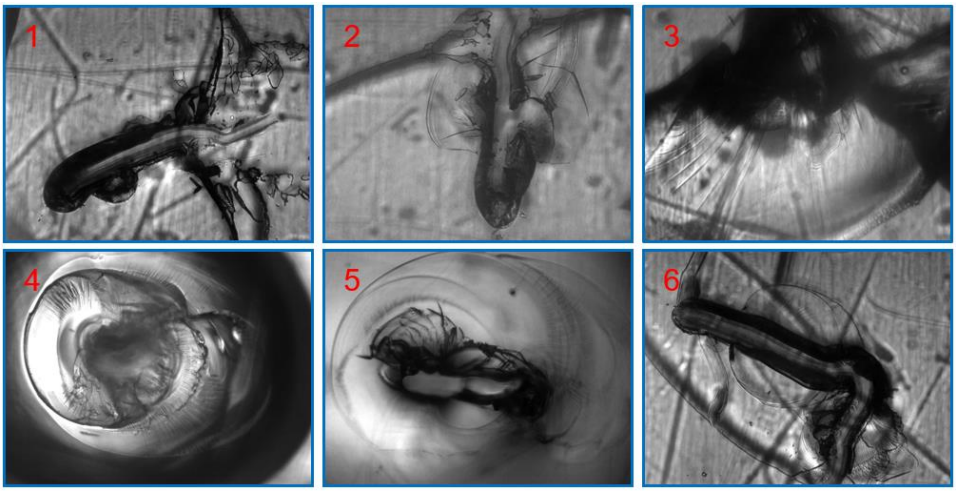

Figure S3. T_g estimation using poke-flow technique. Shattering of GLU/HEX mixture with a mass ratio of 4:1. The shattering temperatures are 247 K, 247 K, 244 K, 253 K, 248 K, 249 K. The average is (248 ± 3) K.

The LEV substrates exhibit more complicated morphological and solidification characteristics. In Fig. S4, in image 1 the film surface is in focus whereas in image 2 the bottom of the substrate is in focus. Those two images demonstrate that the film is transparent. In Fig. S4, image 3, the film was poked and displays semisolid properties at 293 K. One hour later (much longer than the duration of the uptake experiments), the dent is still unchanged as is visible in image 4. Figure S4, image 5, displays crystallization while being poked at 260 K. The crystallization proceeds into the surrounding substrate as displayed in image 6 (10 seconds later). In summary, the LEV substrates exhibit a semisolid or solid phase state in our studied temperature range from 213 K to 293 K. The glass transition mechanism of LEV is beyond the scope of this study and is thoroughly discussed by (Tombari and Johari, 2015) and Lienhard et al. (2012).

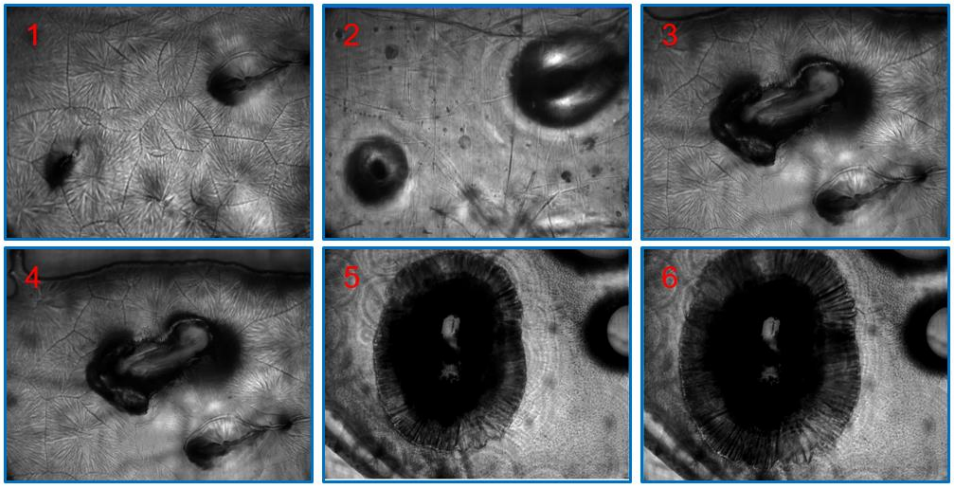

Figure S4. Morphology of LEV at 293 K. Image 1 focuses on film top and image 2 focuses on film bottom. Image 3: substrate poked at 293 K, image 4: the same substrate as image 3 after 1 hour. Image 5: crystallization occurred after poking, image 6: the same substrate as image 5 after 10 s.

Figure S5 displays the highest temperatures under which we observed the shattering of the LEV substrate film yielding T_g = (243 ± 4) K. Figure S5, image 6, shows crystallization of the glassy film presented in image 5 upon warming. Figures S6 and S7 show the poke-flow experiments for LEV/XYL substrate mixtures. In Fig. S6 at 293 K, the LEV/XYL substrate film recovers quickly within 1 min, exhibiting enhanced flow characteristics compared to GLU/HEX films. Figure S7 displays the shattering of the LEV/XYL substrate at temperatures around T_g = (238 ± 3) K.

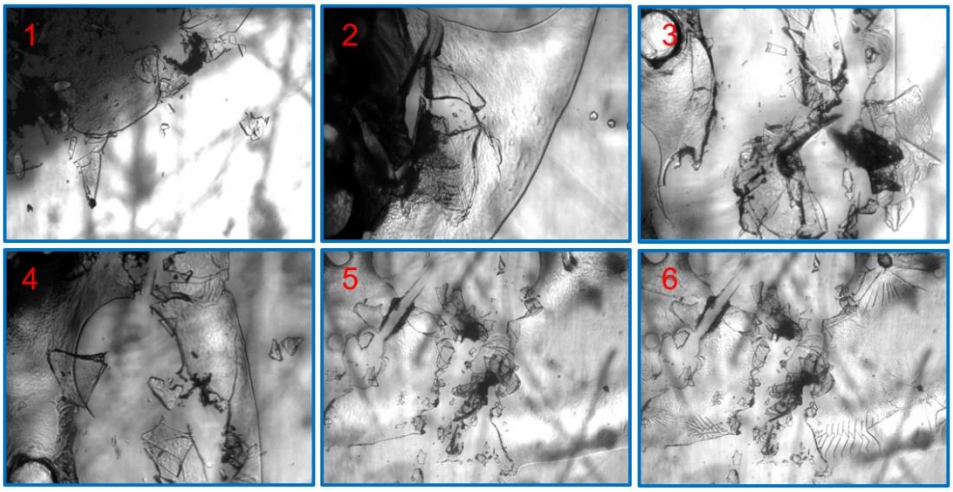

Figure S5. T_g estimation using poke-flow technique. Shattering of LEV in images 1-5. The shattering temperatures are 244 K, 239 K, 237 K, 245 K, 248 K. The average is (243 ± 4) K. Image 6 shows crystallization of substrate film in image 5 upon warming.

140

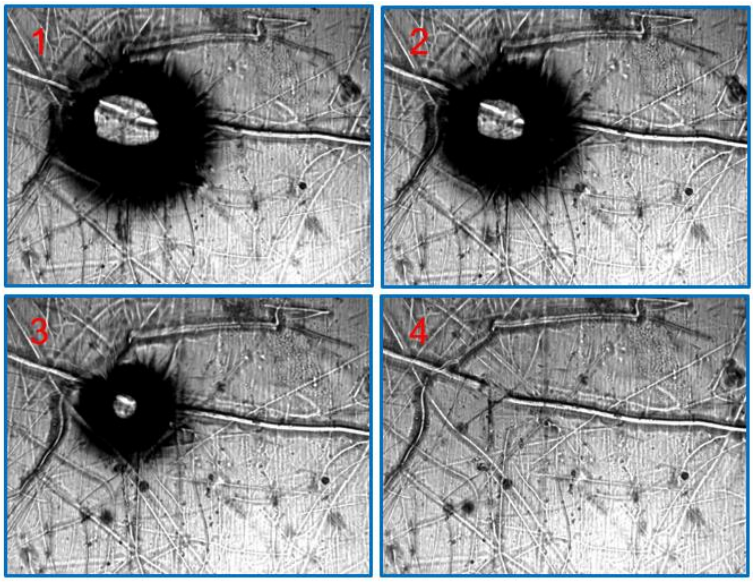

Figure S6. Morphology of LEV/XYL at 293 K. After poking by a needle, the film recovered quickly within about 1 min, indicating that the film was in a liquid phase state.

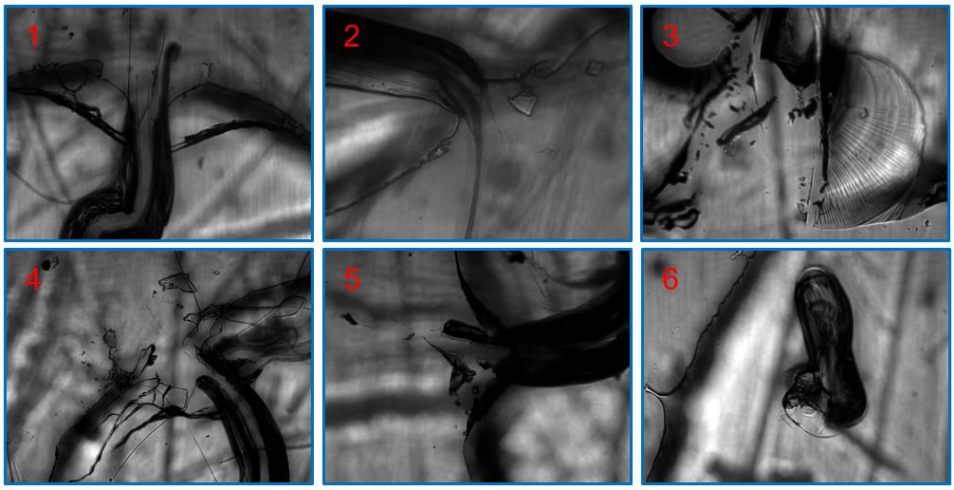

Figure S7. T_g estimation using the poke-flow technique. Shattering of LEV/XYL mixture with a mass ratio of 1:1. The shattering temperatures are 237 K, 236 K, 233 K, 237 K, 240 K, 243 K. The average is (238 ± 3) K.

S4 Surface coverage fraction of unoxidized reaction sites

The fraction of the unoxidized reaction sites (F) on the film surface can be estimated by using the equation below (Bertram et al., 2001):

$$F = \exp\left(\frac{\gamma Z t}{N_{\mathrm{tot}}}\right), \qquad \text{(S2)}$$

where γ represents the uptake coefficient, Z is the collision frequency of the gas oxidant with the surface (molecules $\mathrm{cm^{-2}s^{-1}}$) defined as $Z = [\mathrm{X}]_g \cdot \frac{\omega_X}{4}$, (Pöschl et al., 2007). t is reaction time and N_{tot} is the number concentration of reactive sites ($\mathrm{cm^{-2}}$).

When the substrate films are liquid, the surface can be assumed to be always replenished under our experimental conditions. However, when the substrate films are solid or semisolid, γ may be affected by surface saturation effects, i.e., during the experiment time a significant fraction of the surface reactants are lost. This effect can be avoided either by lowering the oxidant concentration or by shortening the exposure time. A typical reaction time in uptake experiments ranges from 5 to 18 min. As shown in Table S7 below, under the experimental conditions, the substrate surfaces can be considered as fresh surfaces during the reactive uptake kinetics studies. The number concentration of reactive sites is assumed to be 1×10^{15} $\mathrm{cm^{-2}}$ based on the average number of surface reactive sites (Bertram et al., 2001;Shiraiwa et al., 2012). Less than 5% of the substrate

surface area will be oxidized in presented uptake experiments, thus, implying negligible impact of surface saturation effects on the derived kinetics.

Table S7. Estimation of the degree of substrate surface oxidation under typical experimental conditions. Reactive uptake coefficient (γ), gas-phase oxidant concentration $[X]_g$ exposure time (t), number concentration of reactive sites (N_{tot}) and fraction of unoxidized reaction sites (F) are given.

oxidant	γ	$[X]_g$ / molecules cm^{-3}	t / min	N_{tot} / cm^{-2}	F / %
O_3	3×10^{-5}	3×10^{11}	18	1×10^{15}	91.6
NO_3	8×10^{-4}	1×10^{10}	18	1×10^{15}	93.4
OH	0.2	3×10^{7}	18	1×10^{15}	90.6

References

Bertram, A. K., Ivanov, A. V., Hunter, M., Molina, L. T., and Molina, M. J.: The reaction probability of OH on organic surfaces of tropospheric interest, J. Phys. Chem. A, 105, 9415-9421, http://doi.org/10.1021/jp0114034, 2001.

Lienhard, D. M., Bones, D. L., Zuend, A., Krieger, U. K., Reid, J. P., and Peter, T.: Measurements of thermodynamic and optical properties of selected aqueous organic and organic-inorganic mixtures of atmospheric relevance, J. Phys. Chem. A, 116, 9954-9968, http://doi.org/10.1021/jp3055872, 2012.

Lv, X. J., Chen, Z., Ma, J. B., and Zhang, Y. H.: Volatility measurements of 1, 2, 6-hexanetriol in levitated viscous aerosol particles, J. Aerosol Sci, 138, 105449, http://doi.org/10.1016/j.jaerosci.2019.105449, 2019.

Pöschl, U., Rudich, Y., and Ammann, M.: Kinetic model framework for aerosol and cloud surface chemistry and gas-particle interactions–Part 1: General equations, parameters, and terminology, Atmos. Chem. Phys., 7, 5989-6023, http://doi.org/acp-7-5989-2007, 2007.

Shiraiwa, M., Pöschl, U., and Knopf, D. A.: Multiphase Chemical Kinetics of NO_3 Radicals Reacting with Organic Aerosol Components from Biomass Burning, Environ. Sci. Technol., 46, 6630-6636, http://doi.org/10.1021/es300677a, 2012.

Tombari, E., and Johari, G. P.: Structural fluctuations and orientational glass of levoglucosan-High stability against ordering and absence of structural glass, J. Chem. Phys., 142, 104501, http://doi.org/10.1063/1.4913759, 2015.